SANDIA REPORT

SAND 2003-3606
Unlimited Release
Printed Ocotber 2003

Molecular-Scale Studies of Single-Channel Membrane Pores: Final Report

Alan R. Burns, Kervin O. Evans, James G. Fleming, and Brian S. Swartzentruber

Approved for public release; further dissemination unlimited.

Sandia National Laboratories

Molecular-Scale Studies of
Single-Channel Membrane Pores

Alan R. Burns and Kervin O. Evans*
Biomolecular Materials and Interfaces Dept.

James G. Fleming
MEMS Technology S &T Dept.

Brian S. Swartzentruber
Surface and Interface Science Dept.

Sandia National Laboratories
P. O. Box 5800
Albuquerque, NM 87185-1413

*Present address: National Center for Agricultural Research (NCAUR)
                      Peoria, Il

ABSTRACT

We present our research results on membrane pores. The study was divided into two primary sections. The first involved the formation of protein pores in free-standing lipid bilayer membranes. The second involved the fabrication via surface micromachining techniques and subsequent testing of solid-state nanopores using the same characterization apparatus and procedures as that used for the protein pores. We were successful in our ability to form leak-free lipid bilayers, to detect the formation of single protein pores, and to monitor the translocation dynamics of individual homogeneous 100 base strands of DNA. Differences in translocation dynamics were observed when the base was switched from adenine to cytosine. The solid state pores (2-5 nm estimated) were fabricated in thin silicon nitride membranes. Testing of the solid sate pores indicated comparable currents for the same size protein pore with excellent noise and sensitivity. However, there were no conditions under which DNA translocation was observed. After considerable effort, we reached the unproven conclusion that multiple (<1 nm) pores were formed in the nitride membrane, thus explaining both the current sensitivity and the lack of DNA translocation blockages.

Contents

1.0 Introduction

When it was discovered that a voltage gradient across a bilayer system would drive single-stranded polynucleotides through a transmembrane channel (nanopore), a new realm of single molecule detection and characterization was opened. Large, single-stranded biological molecules (i.e. RNA, DNA, or proteins) passing through single ion channels would displace the ions flowing through the channels (Akeson, Branton et al. 1999; Meller, Nivon et al. 2000; Movileanu, Howorka et al. 2000). This ionic displacement would produce a transient blockage of the measured current through the nanopore. The duration of these transient blockages was found to be proportional to the length of the molecule (Kasianowicz, Brandin et al. 1996). Studies have also shown that single molecules of homonucleotides could be distinguished from one another by their sequence-dependent displacement of the current (Akeson, Branton et al. 1999), (Meller, Nivon et al. 2000). Our approach in this field has been to move from the protein nanopore to more robust solid-state nanopores, created with silicon micromachining techniques.

The well-studied α-hemolysin toxin (cited above) was chosen as our model nanopore system. It is a water-soluble protein secreted by *Staphylococcus aureus* bacilli. This protein toxin is a single monomer consisting of 293 amino acids and approximately 33 kDa in size. α-hemolysin toxin forms an heptameric (7 units, see figure 1) water-filled ion channel in a lipid bilayer membrane. The heptameric pore complex is shaped like a mushroom that is 100 Å in height and up to 100 Å in outer diameter. The section of the toxin above the membrane is approximately 70 Å long. As shown in figures 1 and 2, the aqueous channel spans the thickness of the bilayer (~52 Å), and its inner diameter ranges

Figure 1. Side view of ribbon representation of the α-hemolysin heptameric pore with each monomer highlighted in a different color (Song, Hobaugh et al. 1996).

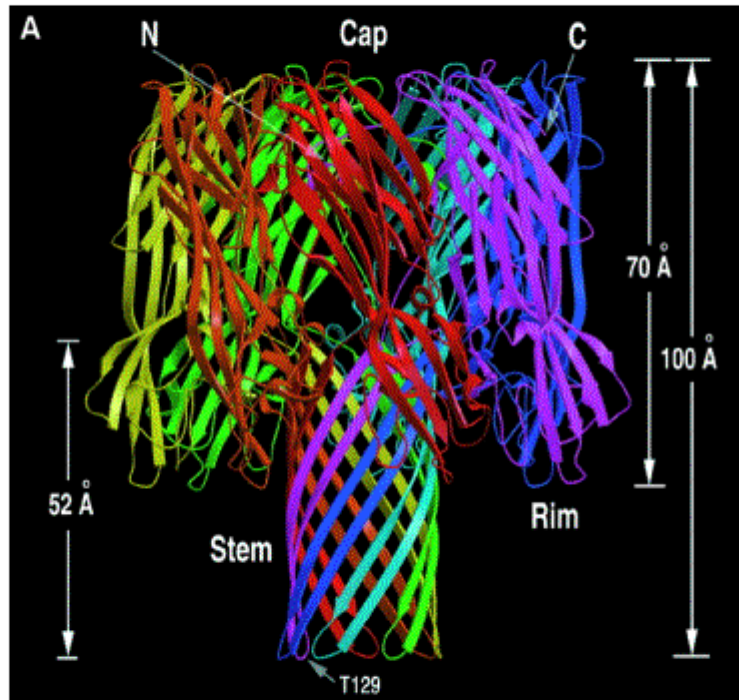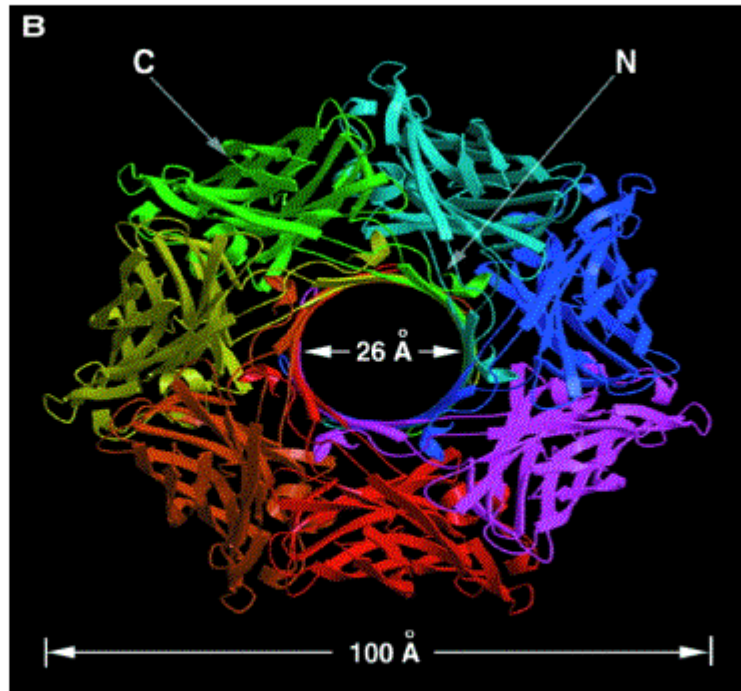Figure 2. Top view of ribbon representation of the α-hemolysin heptameric pore with each monomer highlighted in a different color (Song, Hobaugh et al. 1996).

from 14 Å to 46 Å (Song, Hobaugh et al. 1996). As a nanopore, α-hemolysin remains open unless it is blocked by other biomolecules.

Our work encompassed three areas of nanopore research. The first area was to use the α-hemolysin toxin as the model system through which to establish baseline capabilities with single-nanopores and single molecule detection. The second area of interest was characterizing solid-state nanopores that mimicked the α-hemolysin toxin. Finally, we used our single ion channel system to characterize tetanus toxin as a nanopore system.

2.0 Materials and Methods

2.1 *Materials*

Lipids (1,2-diphytanoyl-*sn*-Glycero-3-phosphatidylcholine [DPh-PC], 1,2-distearoyl-*sn*-Glycero-3-phosphatidylcholine [DSPC],) and cholesterol (chol) were purchased as dried powder from Avanti Polar Lipids, Inc. without further purification. Lipids were generally stored in chloroform at –20˚C. Receptor lipids such as monosialoganglioside-GT1b were purchased from Sigma Chemical Company (St. Louis, MO), without further purification. Receptor lipids were stored in a chloroform/methanol mixture at 2:1 ratio.

Water used in all experiments was purified using a Barnstead ultrapure reversed osmosis system to give high resistivity ≥ 17.8 MΩ-cm. All organic solvents (ethanol, hexane, hexadecane, chloroform, methanol) were purchased from Fisher Scientific Company, ACS grade or better. Also, sodium chloride, potassium chloride, sodium hydroxide, potassium hydroxide, glycerol, cobalt chloride, ethylenediaminetetraacetic acid (EDTA), glycerol, and tris(hydroxymethyl)aminemethane [Tris-HCl] were

purchased from Fisher Scientific Company at ACS grade or better. 2-[4-(2-Hydroxyethyl)-1-piperazine]ethanesulfonic acid [HEPES] was purchased from Acros Organics. Sequences of DNA were purchased from Sigma-Genosys (Woodlands, TX) as desalted powders at 0.05- or 0.2-μM concentration. The fluorescent probe calcein was purchased from Molecular Probes, Inc. (Eugene, OR). All chemicals were used without further purification.

α-hemolysin toxin was purchased from Calbiochem (now EMD Sciences, San Diego, CA) or List Laboratories, Inc. (Campbell, CA). The tetanus toxin and its C-fragment were purchased from Calbiochem. No further purification was done.

DNA was stored dry in the freezer at –20 ℃ until needed. For experiments, DNA was rehydrated in 400 μl of buffer (1 mM EDTA, 10 mM Tris-HCl, pH 8 ± 0.05) and kept on ice. Otherwise, rehydrated DNA was kept in the refrigerator at 4 ℃.

2.2 Methods

2.2.1 *Single toxin ion-channel chamber*

The single-ion-channel chamber for toxin nanopores was a Teflon® shell with two wells connected by Teflon® tubing. The connecting Teflon® tubing was a piece of tubing (~1–1.25 inches long) with shrink-wrap Teflon® melted to form a cap (figure 3). Free-standing lipid bilayers (discussed below) were formed across a well-defined orifice in the shrink-wrap cap created by gently pushing a 25 μm steel stylus through the cap as the shrink-wrap was reheated.
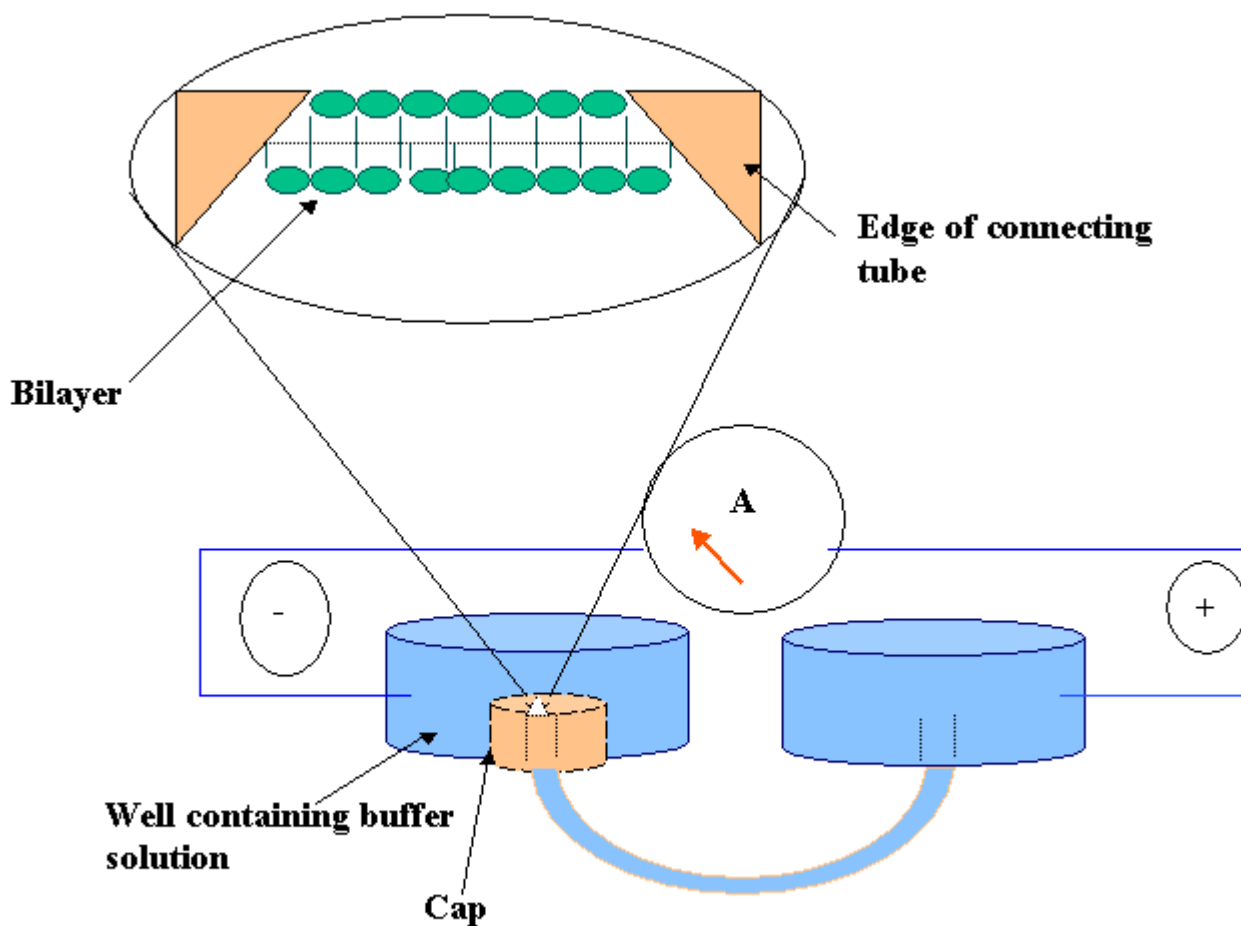
Figure 3. General set up of single-ion-channel chamber. Teflon® tubing with a shrink-wrapped cap connects two separate reservoirs. At the end of the cap is the orifice where bilayers are formed. The *cis* reservoir is on the left; the *trans* reservoir is on the right.

The single ion channel chamber for toxin nanopores was cleaned in boiling nitric acid (~15 - 25% v/v) for approximately 20 minutes prior to each experiment. Once the chamber cooled, it was rinsed three times in nanopure water. The connecting tube was then flushed with ≥ 150 µl of water, ethanol, and hexane each. After each solvent flush, air was then drawn through the connecting tube to dry it.

2.2.2 *Formation of free-standing lipid bilayers*

It was found that a bilayer was stable for longer periods of time if a thin film of lipids were dried inside the tubing to "pre-coat" the orifice. Therefore, lipids for coating the tube were prepared by placing 50 µl of stock DPh-PC (10-µg/µl) in a culture test tube followed by gentle drying with a stream of nitrogen. These lipids were rehydrated in 250 µl of hexane and capped for later use. The connecting tube was coated with lipids by allowing 5 µl of the coating lipids to wick into the tubing. Air was then forced through the tubing to dry the hexane, leaving a thin film of lipids inside the tubing and possibly outside of the cap. After 5–15 minutes of further drying, buffer solution was slowly forced through the tubing to fill it and the two wells. A bubble-free tube was confirmed by the "seal test" on the amplifier was turned on. The seal test refers to applied square-wave signal across the cell. A full square wave in current indicated free flow of current (positive) ions from the *trans* to *cis* reservoirs (see figure 4). A differentiated square wave (transient spikes ~600–1000 pA) occurs when the lipid bilayer is present (discussed below) or there is a bubble in the tube (see figure 5).

Once the wells on the chamber were filled with buffer, a bilayer was formed across the orifice. To create a bilayer, the lipids were prepared by placing 15 µl drop onto
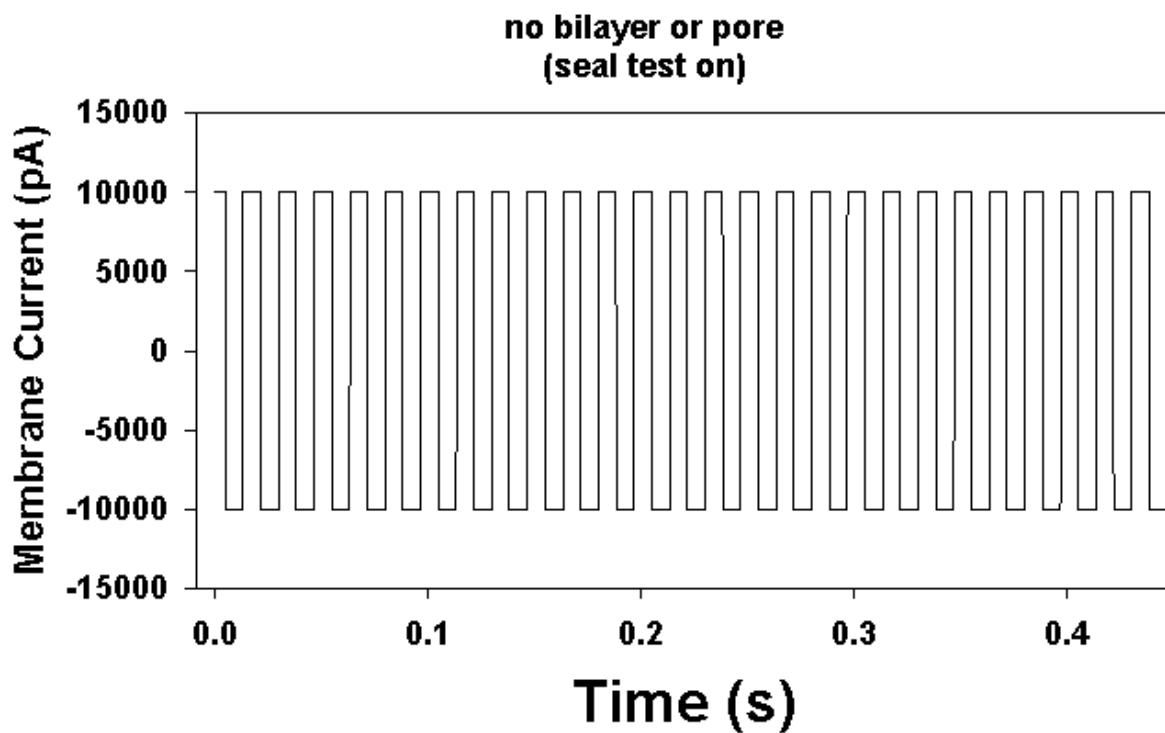
Figure 4. This is the electrical signal due to an applied square wave "seal test" in the case of free flow of current. Thus there is no bilayer or air bubble in the tube. The seal test was run at 5 mV / 8 ms.
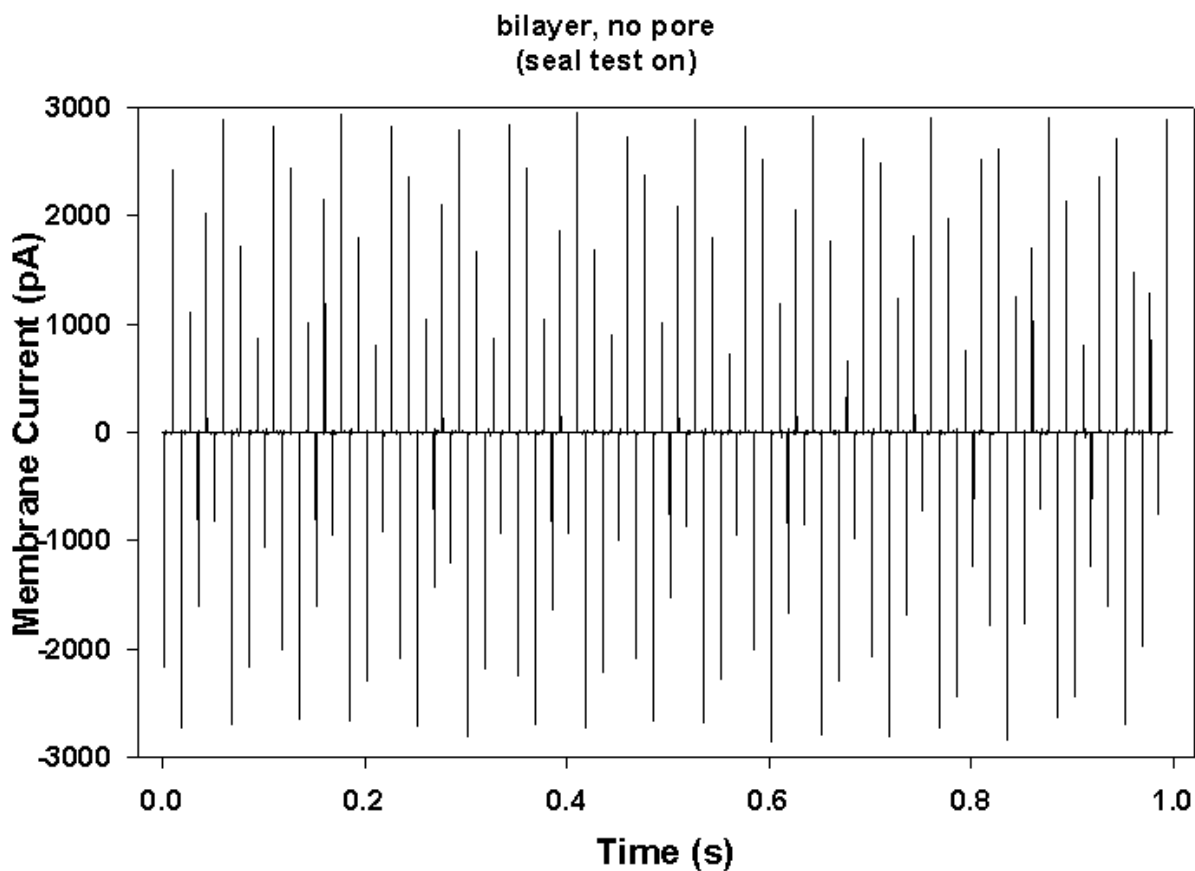
Figure 5. Electrical signal due to an applied square wave "seal test" in the case where a thin free-standing DPh-PC bilayer is present. The square wave (figure 4) becomes transient spikes $\geq 2000 \pm 200$ pA when a bilayer thins over the orifice of the single-ion-channel chamber. Thus we know when the bilayer is established and can measure its capacitance. The later is maximum when the membrane is "thinned" of all organic solvent and is ready for a pore. The impedance of a leak-free bilayer exceeds 10 GΩ.

a glass slide and allowing it to air-dry. Next, a pipette with a disposable tip attached was dipped into hexadecane just so that the solvent wicked into the tip (≤ 1 µl). This aliquot of solvent was placed onto the glass slide away from the dried lipid spot. After wiping the pipette tip to remove excess hexadecane, the tip was dipped into the solvent aliquot to remove a smaller amount and that was thoroughly mixed with an edge of the dried lipid spot. This was continued until a small amount of lipid and solvent formed a paste and a small amount was transferred onto the tip. Finally, "lipid bubbles" were blown across the orifice until the above square wave (figure 4) became transient spikes (figure 5). The transient spikes were the discharging signal of the bilayer, which acted as a capacitor. Therefore, the thinner the bilayer became the larger the capacitance became. Typically, functional thin bilayers had transient spikes that peaked $\geq 2000 \pm 200$ pA (figure 5); anything less was usually an indication that the organic solvent used to "paint" the bilayer was still in the middle of the bilayer and had to be removed by diffusion. Bilayers were allowed to settle for $5 - 15$ minutes before adding toxin to form a single nanopore.

2.2.3 *Single-channel protein pore formation*

 α-hemolysin was stored in 1:1 glycerol/water mix at 0.5 µg/µl prior to use. For each experiment, 10 µl of toxin was aliquoted to an eppendorf tube, mixed with 90 µl of 1 M KCl, 10 mM HEPES buffer at pH 8 ± 0.05 to give an experimental concentration of 0.05 µg/µl, and stored on ice during the experiment. The same buffer was used for all DNA translocation experiments. Toxin was added typically $1 - 2$ microliters at a time to the *cis* well. The current across the membrane was now monitored in DC mode with an applied potential of -120 mV (*trans* well grounded). Typical currents across a bilayer of

diphytanoyl phosphatidylcholine (DPh-PC) before nanopore formation were <3 pA (basically in the noise) and completely featureless. Once a *single* nanopore of α-hemolysin toxin was established, as indicated by a sudden stepwise increase in current to ~ 120 pA, the excess toxin was carefully flushed out (so as not to rupture the membrane) with 3 – 5 ml of buffer. (An example of the step-wise increase in current due to the formation of a *second* pore is shown later on in figure 12). Established single nanopores were allowed to settle for 5 minutes before single stranded DNA was introduced into the *cis*-well (negative electrode) for translocation studies. In a typical experiment, DNA was added at a final concentration of 2.5-μM.

With the *cis* well negative, typically 120 mV was applied such that a positive current was detected when a nanopore opened. Current measurements were measured using a patch-clamp amplifier and head-stage (Axopatch 200B and CV203BU, Axon Instruments, Foster City, CA). The amplified signals were low-pass filtered at 5 kHz and digitized (at 250 kHz for α-hemolysin, 20 kHz for tetanus) with a Digidata 1320A from Axon Instruments.

2.2.4 *Chamber for Solid-State Nanopores*

The chamber for solid-state nanopores (described below) was analogous to the one used for membrane protein pores discussed above. The solid-state nanopore chamber (figure 6) was a Teflon® shell with two wells connected by a trench instead of the Teflon® tube. Midway across the trench was a slit for mounting the solid-state nanopores. Rinsing with distilled water, soaking in hexane and drying with a stream of nitrogen were performed to clean the chamber prior to mounting a nanopore in the
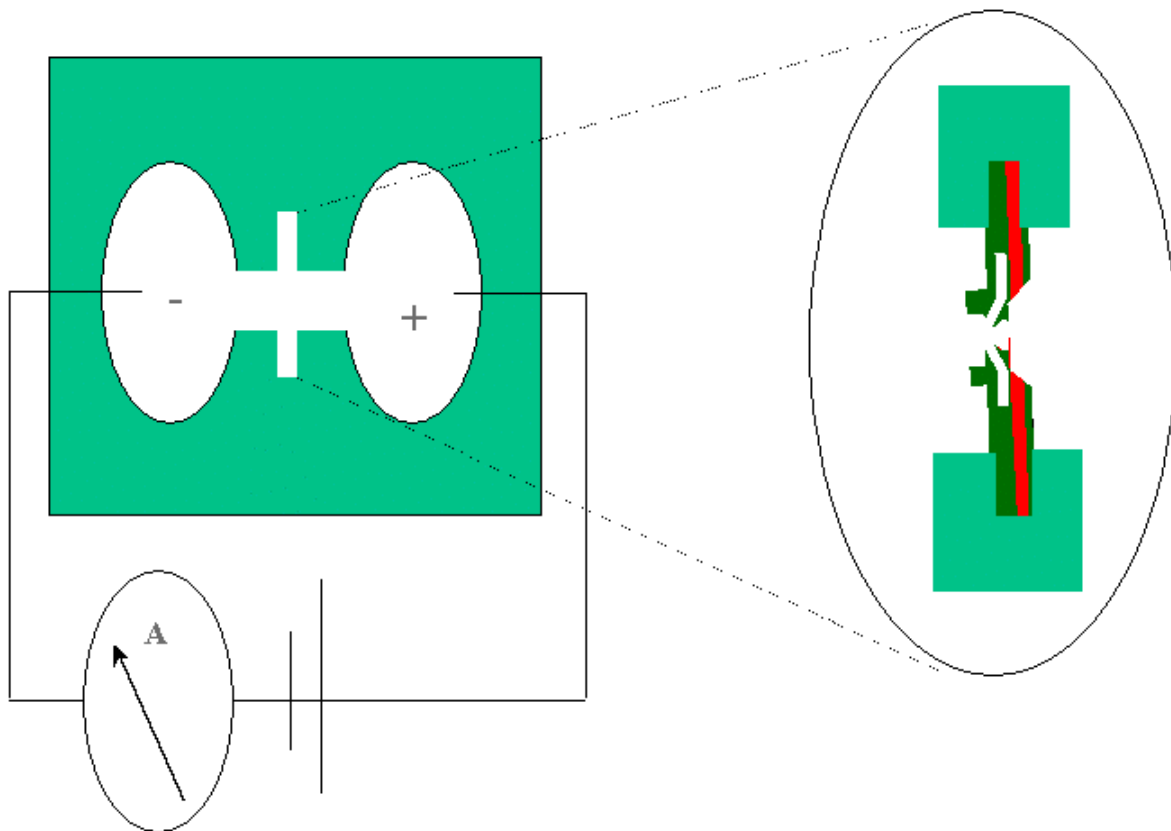
Figure 6. The solid-state nanopore chamber. The chamber is made of a Teflon® piece with two reservoirs connected by a trench. The solid-state nanopore is sealed into a slit that nearly bisects the trench.

chamber. Leak-free seals were accomplished by placing Sylgard 170 sealant in small amounts around the edges where the nanopore met the Teflon® chamber. The buffer was the same as for the protein nanopore experiments. The *cis* well generally was the one with the wider opening over the nanopore that was etched in the center of the nanopore chip. The electronic setup was the same as for the toxin nanopores, except filtering was done at 1 or 2 kHz, and digitizing done at 10 kHz.

2.2.5 *Solid-State Nanopore Fabrication*

The fabrication process for the solid-state nanopores was based on work at Stanford (Liu, Biegelsen et al. 1993) that found that narrow pillars of silicon exhibited a self-limiting oxidation behavior under certain conditions. For instance, the self-limiting oxide thickness of a 20 – 50 nm silicon core was 2 – 5 nm. Thus we sought to utilize this process to make *single* 2-5 nm pores in a silicon nitride (Si_3N_4) "membrane." Fabrication was begun by chemical vapor deposition of silicon nitride (Si_3N_4, green) onto a thick layer (~ 200 – 500 nm) of polysilicon (figure 7a). Then a layer of silicon dioxide (SiO_2, figure 7a) was deposited onto the silicon nitride. After reactive-ion etching was done to pattern the silicon nitride and silicon dioxide (figure 7b), isotropic wet etching was done in phosphoric acid to further cut the silicon nitride (figure 7c). Transmission electron microscopy (TEM) images showed that the silicon nitride was undercut to about a third the size of the silicon dioxide layer (~ 100 nm; figure 8). Hydrofluoric acid (HF) was then used to strip away the SiO_2 (figure 7d), followed by a combination of isotropic and anisotropic etches to form a tip in the polysilicon layer (figure 7e). Oxidation was then

a — Chemical vapor deposition of silicon nitride (Si$_3$N$_4$, green), then silicon dioxide (SiO$_2$, blue) onto a thick layer of polysilicon (red).

b — Reactive-ion etching (RIE) to pattern the Si$_3$N$_4$ and SiO$_2$.

c — Isotropic wet etch of Si$_3$N$_4$ in phosphoric acid.

d — Hydrofluoric acid (HF) used to strip away SiO$_2$.

e — Combination RIE isotropic and anisotropic etches to form "tip".

f — Oxidation to sharpen "tip".

g — RIE to remove Si$_3$N$_4$.

h — Second polysilicon layer deposited.

i — RIE to pattern second polysilicon layer.

j — HF etching to remove all SiO$_2$.

k — Chemical vapor deposition of Si$_3$N$_4$.

l — RIE to pattern Si$_3$N$_4$.

m — Chemical vapor deposition of thin layer of Si$_3$N$_4$ on bottom.

n — RIE to pattern Si$_3$N$_4$.

o — Partial KOH etch to slice into the polysilicon.

n — Thinning of Si$_3$N$_4$ in phosphoric acid.

q — Complete KOH etch to form final nanopore.

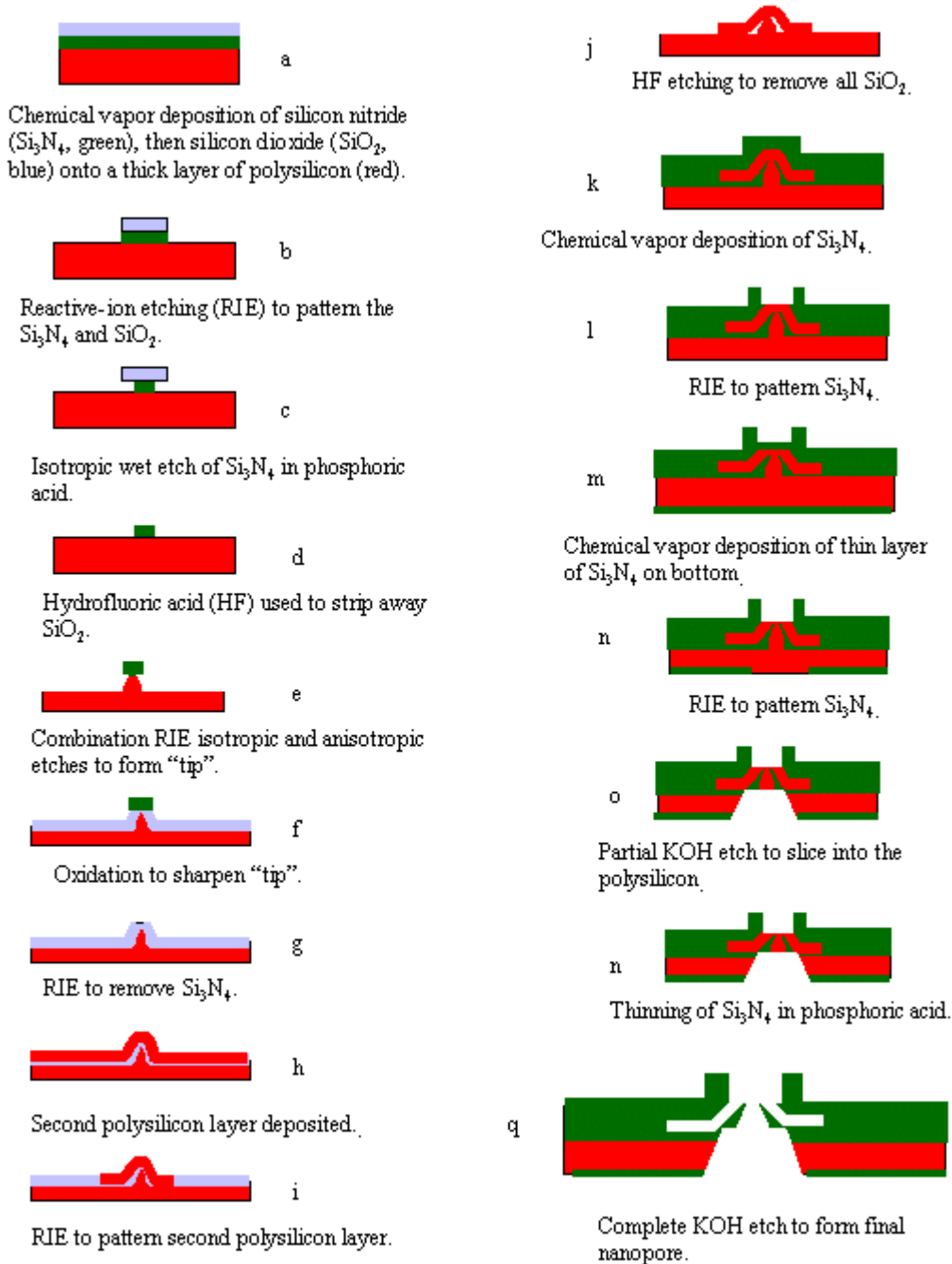Figure 7. Solid-state nanopore fabrication process. The solid-state nanopore was fabricated using chemical vapor deposition (CVD) and reactive-ion etching (RIE) techniques to form a hole 2 – 5 nm across in a film of silicon nitride (S$_3$N$_4$). *Note*: figure is not to scale.
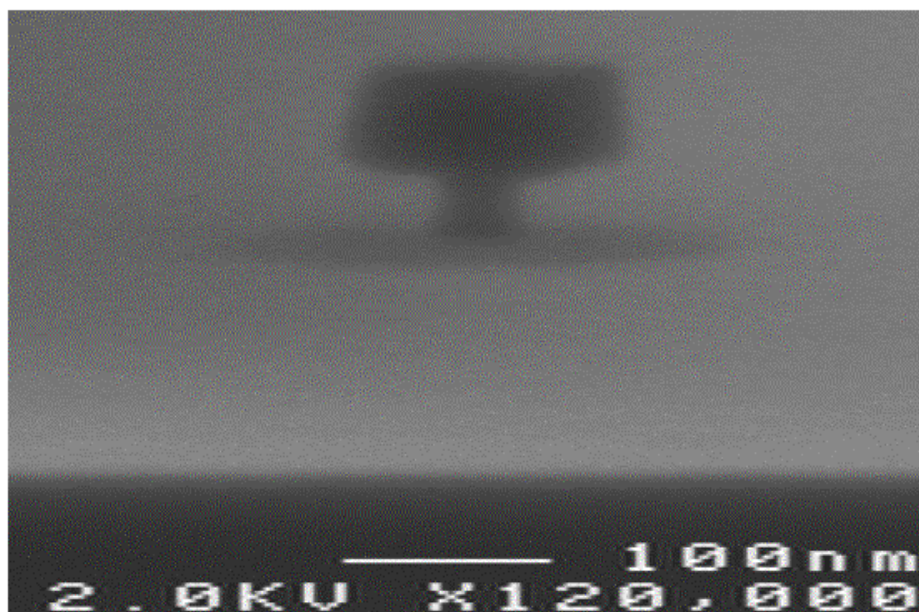
Figure 8. Transmission electron microscopy image of the solid-state nanopore after an isotropic wet etch in phosphoric acid (see figure 7c).

done to sharpen the tip under the Si_3N_4 (figure 7f) and phosphoric acid was used to remove the Si_3N_4 (figure 7g). This was followed by deposition of a second layer of polysilicon (figure 7h) and reactive-ion etching to pattern this second polysilicon layer (figure 7i) (TEM images showed the patterned polysilicon to be 250 – 300 nm across at the base; figure 9). Following etching in HF to remove all of the SiO_2 (figure 7j), Si_3N_4 was layered over the polysilicon by chemical vapor deposition (figure 7k). Reactive-ion etching was done to pattern the Si_3N_4 (figure 7l) so that a hole ~ 100 nm across was etched into the Si_3N_4 (figure 10). A thinner layer of Si_3N_4 was then deposited on the underside of the polysilicon using chemical vapor deposition (figure 7m). Reactive-ion etching was used to cut into the Si_3N_4, exposing the polysilicon layer (figure 7n). A partial potassium hydroxide (KOH) etch used to slice into the polysilicon down to the Si_3N_4 surface (figure 7o). The thicker layer of Si_3N_4 was thinned in phosphoric acid (figure 7p). Finally, a complete KOH etch was done to form a final nanopore structure in the Si_3N_4 (as shown in figure 7q). Note that the figure is not to scale. The final nanopore was 2- 5 nm in diameter, comparable to the α-hemolysin protein pore.
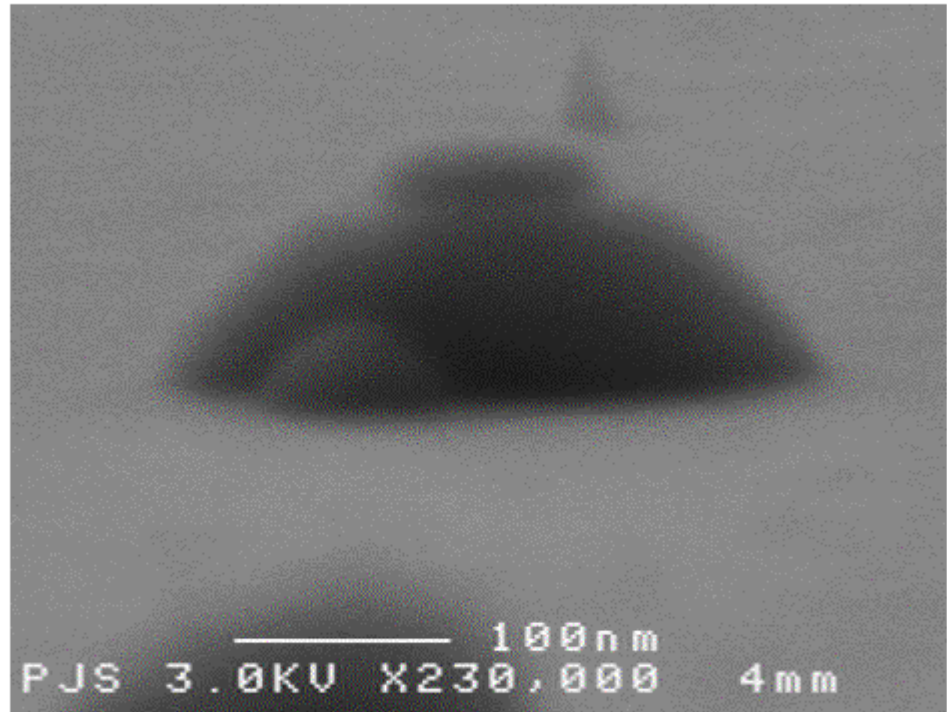
Figure 9. Transmission electron microscopy image of solid-state nanopore after reactive-ion etching to pattern second layer of polysilicon (see figure 7i).
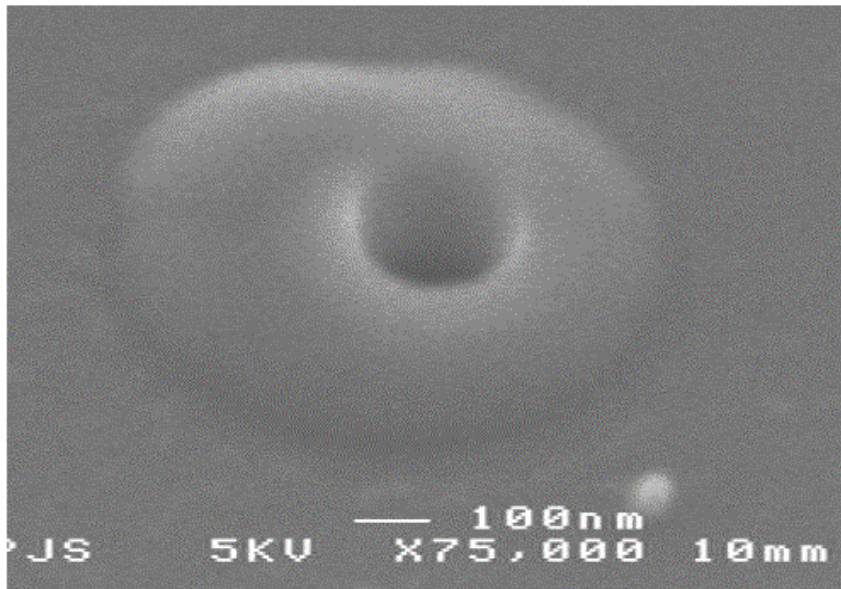
Figure 10. Top view of transmission electron microscopy image of the solid-state nanopore after reactive-ion etching to pattern the top layer of silicon nitride (see figure 7l).

3.0 Results

3.1 *DNA translocation through single protein pores*

Following initial set up of our single-channel system, we were able to establish that we could readily detect single and multiple ion channels of α-hemolysin as they formed in a thin bilayer of DPh-PC. Typically, currents of 120 ± 20 pA were detected for a single pore when $+120$ mV was held across the bilayer. The current (within ± 20 pA) was directly proportional to the applied voltage (figure 11). Also, a single pore was found to be stable for as long as 180 minutes after formation in a bilayer; typically a pore was stable for 90 minutes. Current values were step-wise and linearly cumulative if more pores were allowed to form (figure 12).

After the addition of poly-dA$_{100}$ (single-stranded DNA fragments composed of 100 adenines) to the *cis* reservoir, we soon observed single blockages of the pore by individual molecules of DNA (figure 13). These blockages reduced the current of the pore by 20 to $\geq 70\%$. Analysis of the blockages revealed three ranges of current blockage durations (figure 14). In the first one, DNA reduced the current to $50 - 71\%$ of the fully open pore. The majority of these single strands of DNA passed through the nanopore in less than one millisecond. A second region of blockages ranged from $36 - 50\%$ of the fully open pore. These DNA molecules took as long as 4 ms to transverse the pore. The final range of blockages occurred from $4 - 36\%$ of the fully open pore. These blockages lasted as long as 8 milliseconds. When we repeated the experiments with single-stranded poly-dC$_{100}$ (100 cytosines), we found some interesting differences. When passed through a` single nanopore under the same conditions, it exhibited only two
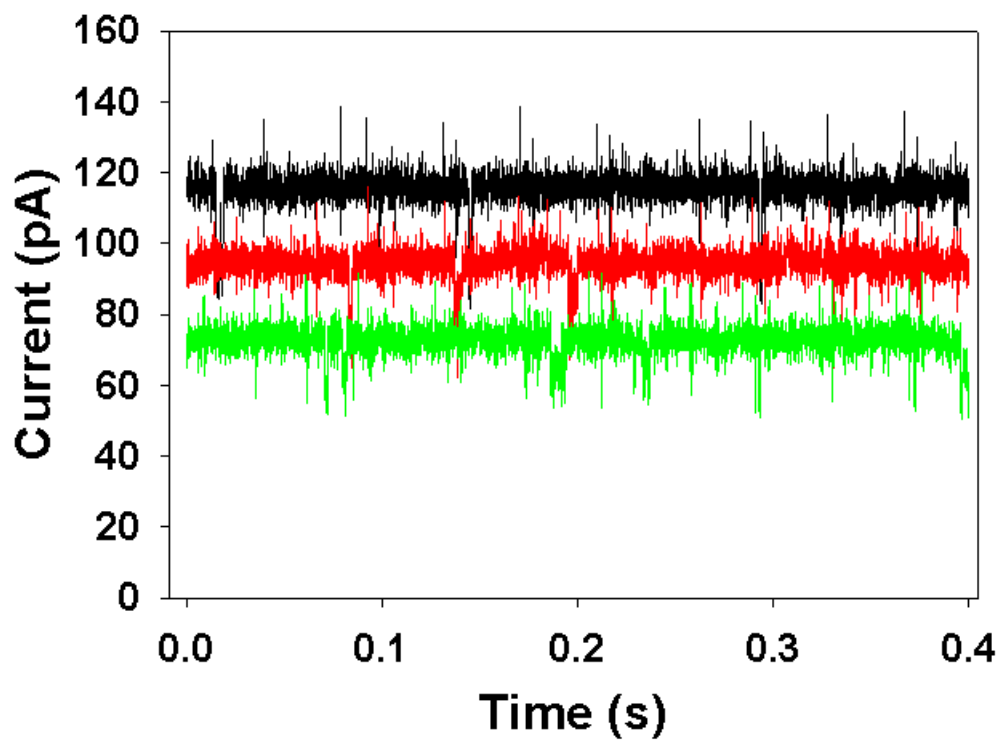
Figure 11. A single α-hemolysin nanopore as a function of voltage. The buffer contained 1 M KCl, 10 mM HEPES at pH 8.
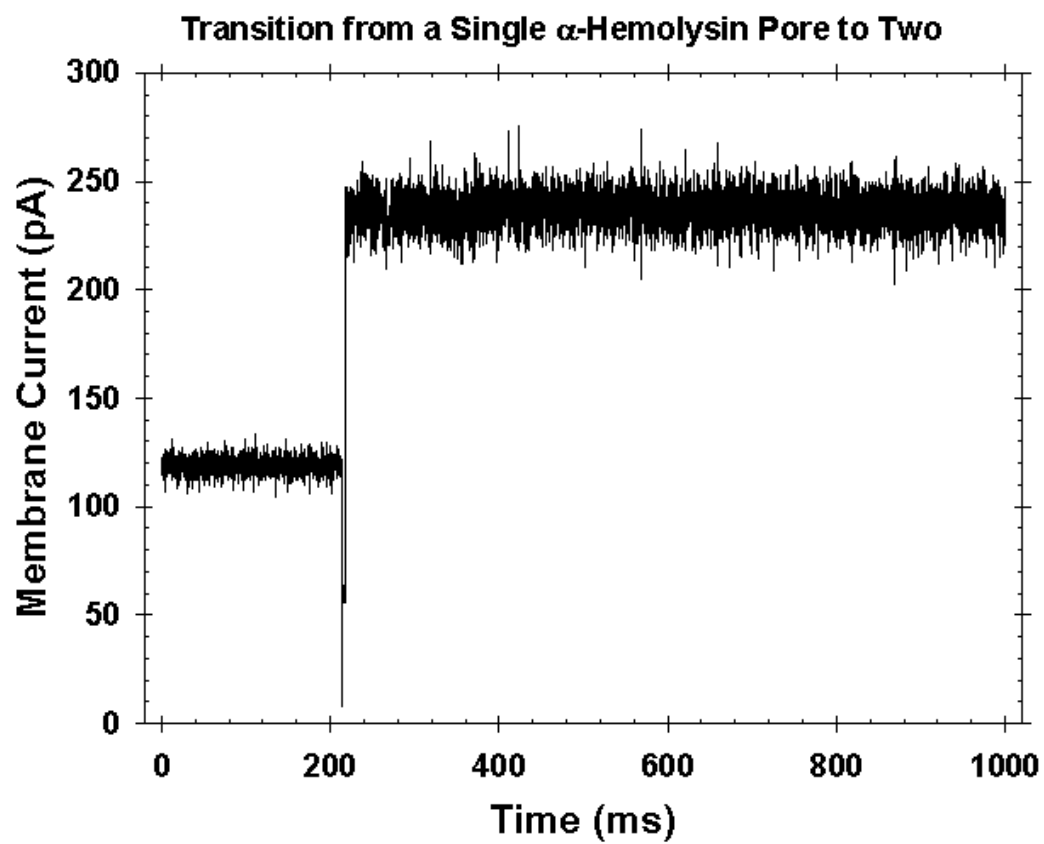
Figure 12. The transition from a single α-hemolysin pore to two. The current due to both nanopores was cumulative. The buffer used contained 1 M KCl, 10 mM HEPES at pH 8. The voltage was +120 mV, filtered at 5 kHz.
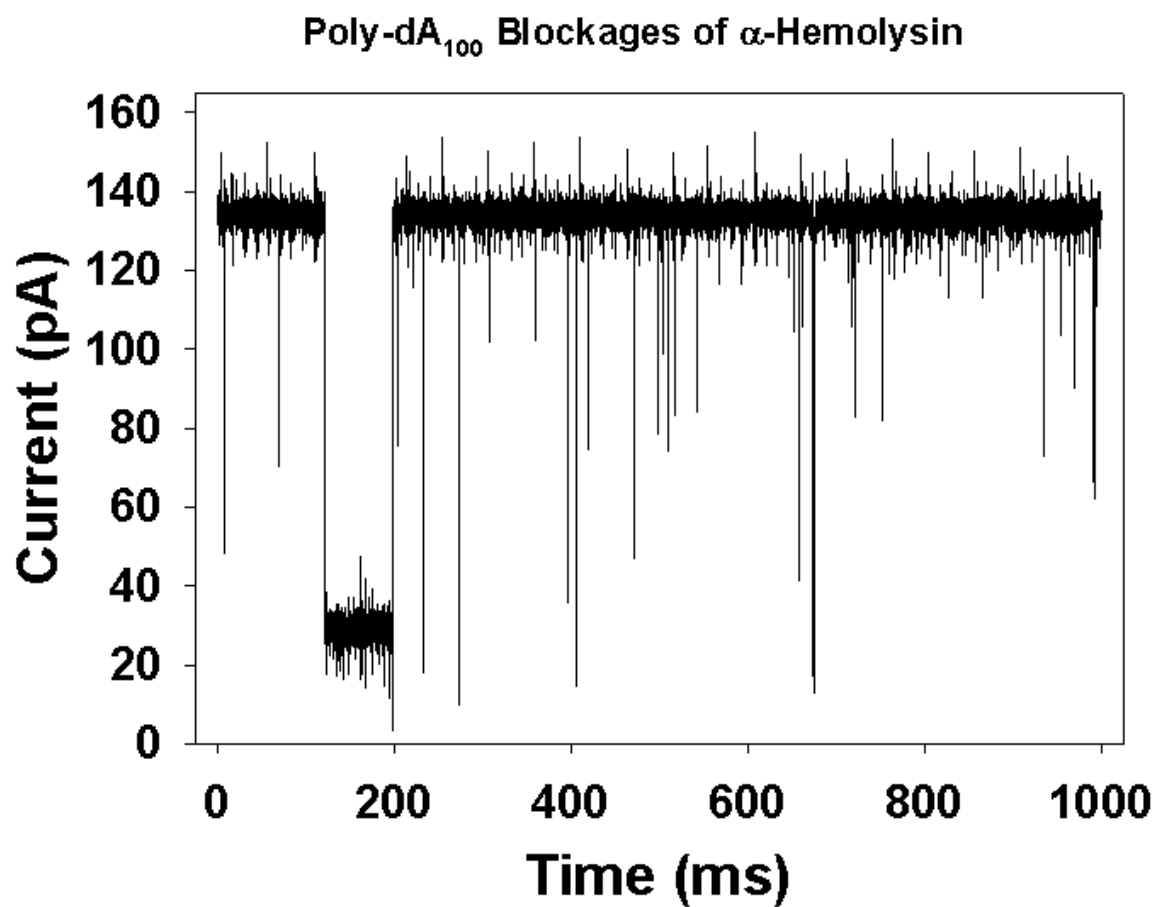
Figure 13. Blockages of a single α-hemolysin pore by homonucleotides poly-dA$_{100}$. The buffer contained 10 mM HEPES, 1 M KCl at pH 8.

ssDNA Blockages of Single α-Hemolysin Pore
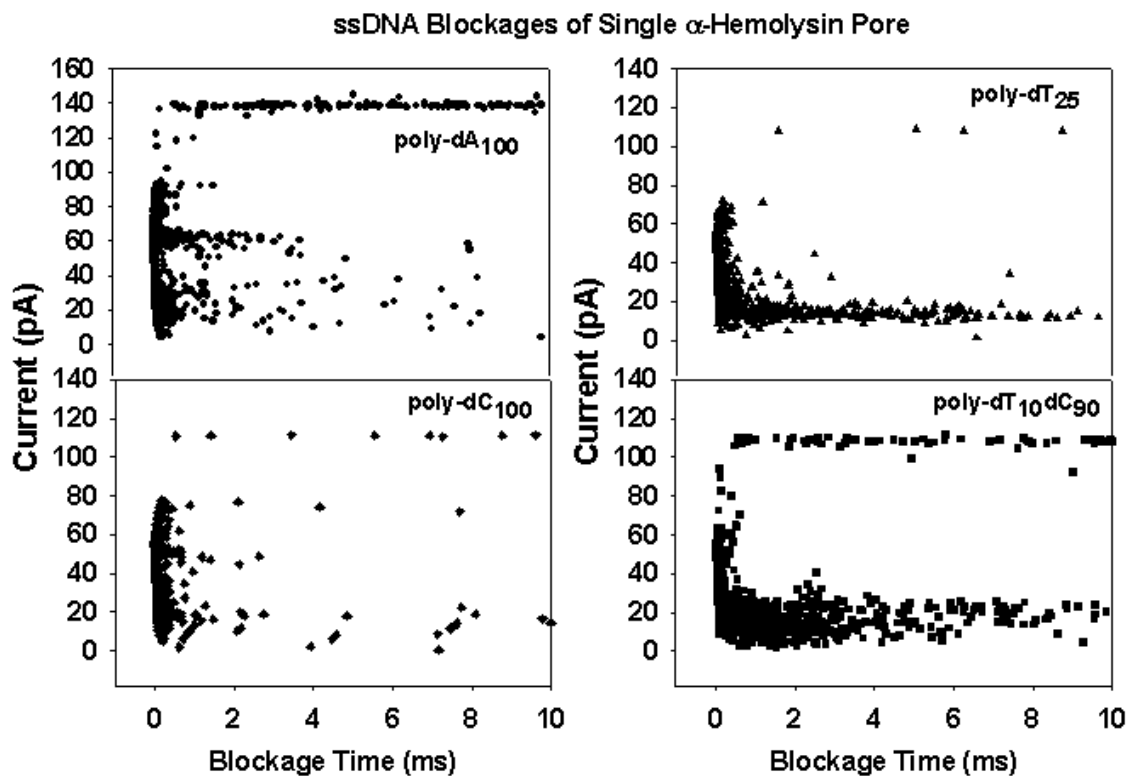
Figure 14. Blockages of a single α-hemolysin pore by single strands of DNA. The DNA used was poly-dA$_{100}$ (circles), poly-dC$_{100}$ (diamonds), poly-dT$_{25}$ (triangles), and poly-dT$_{10}$dC$_{90}$ (squares). The buffer contained 1 M KCl, 10 mM HEPES at pH 8; the voltage was +120 mV.

distinct type of blockages. The first type covered a range of 41–73% of the fully open

pore; the second type ranged from 5 – 36% of the fully open pore. However most of the

blockages in both regions occurred in less one millisecond (figure 14). Unfortunately,

the time range of these two different polymers of homonucleotides did not allow us to

fully distinguish each in a 1:1 mixture.

During our research, however, we did come across literature data that showed that

single-stranded poly-dT_{100} (100 thymines) exhibited the most distinctive blockages of any

single strand of DNA of 100-nucleotide long (Kasianowicz, Henrickson et al. 2001).

Poly-dT_{100} typically created a double blockage as it passed through a hemolysin pore.

The initial blockage reduced current to about 25% of the fully opened pore. This was

followed by a shorter blockage of lesser current (~5–10% of the fully opened pore; figure

15). This type of current blockage was also observed in shorter sequences. We then

decided to measure the blockages if the homopolymer poly-dT contained only 25

nucleotides, just enough to span the entire nanopore (~100 Å).

As figure 15 shows, poly-dT_{25} also exhibited two regions of blockages. One set

of blockages ranged from 41 – 73% of fully open pore, where the blockages occurred in

less than one millisecond. The majority of blockages fell in the second range of 5 – 36%

of the open pore, and took as long as 9 milliseconds. We then wanted to see how

replacing ten cytosines in poly-dC_{100} with poly-dT_{10} (just long enough to stretch from the

limiting vestibule of the nanopore to the end that protrudes out of the bilayer) would

affect the blockages.   As the data show, the blockages resembled those for poly-dT_{25},

except there was a distribution of blockages in the 5 – 36% range that lasted longer than

one millisecond (figure 14). The typical blockage also was similar to that seen when only
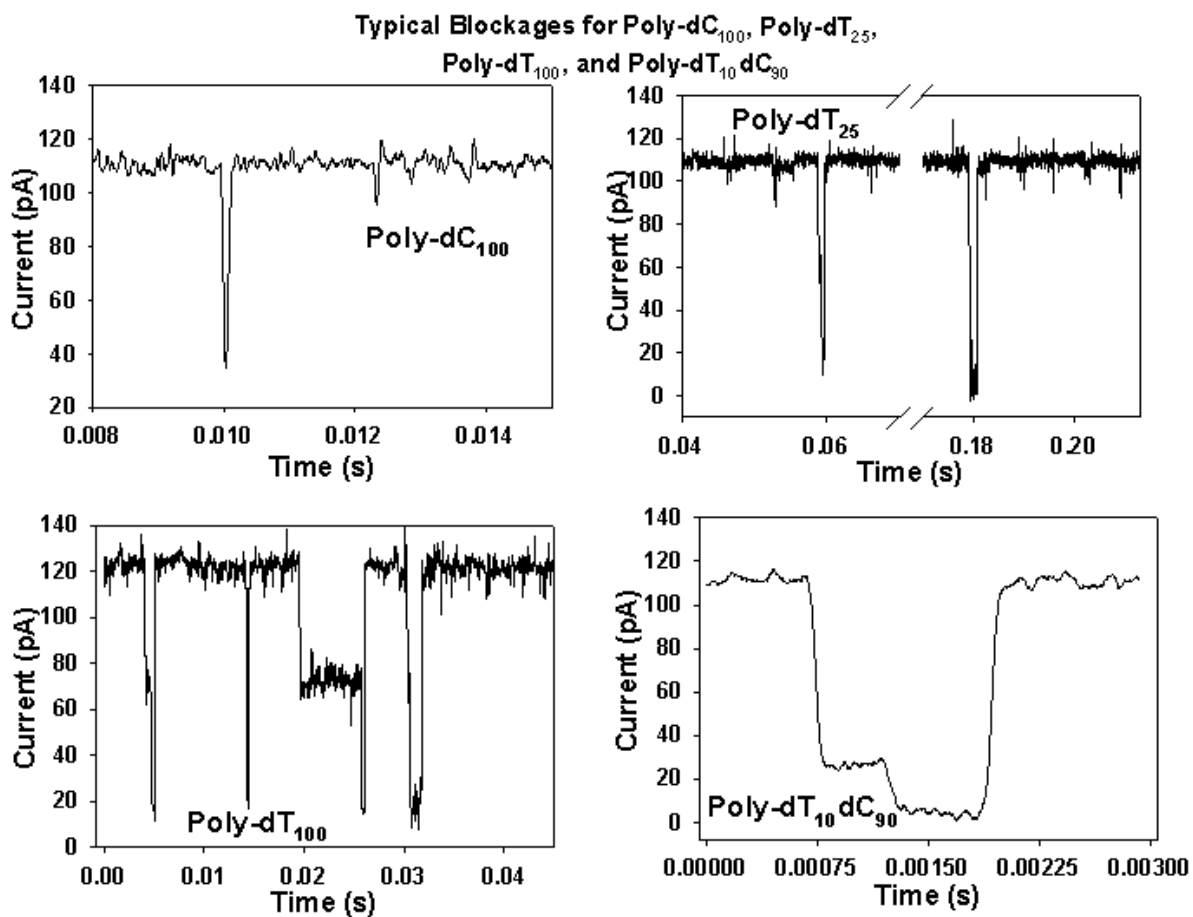
Figure 15. Typical blockages exhibited by poly-dC$_{100}$, poly-dT$_{100}$, poly-dT$_{25}$, and poly-dT$_{10}$dC$_{90}$. By replacing 10 cytosines in poly-dC$_{100}$ with thymines, we were able to change the typical blockage pattern into a pattern that was more intermediate of the two distinct patterns.

poly-dT$_{25}$ or poly-dT$_{100}$ was present in the experiment.

To understand these results in terms of translocation dynamics, the DNA must orient itself into space-filling structures to effectively reduce the current in the protein nanopore since current is reduced primarily when ions are displaced in the limiting section of the protein nanopore. This would mean that if each homonucleotide strand (poly-dA$_{100}$, poly-dC$_{100}$, etc.) of DNA filled the space in the nanopore differently, then the reduced current would be distinctive to that sequence of DNA. This also would mean that the time of the blockages would depend on the amount of space that the DNA strand filled in the nanopore. Particularly, if the DNA filled more space in the limiting section of the nanopore, the DNA was more likely to "brush" against the sides. This would effectively increase the time of the blockage. Akeson et al clearly demonstrated this with RNA sequences of poly-C$_{100}$, poly-A$_{100}$, and poly-dC$_{100}$ (Akeson, Branton et al. 1999). Akeson et al surmised that poly-A$_{100}$ forms a helical structure in solution and starts to unravel as it is pulled through the nanopore (the helical structure is what caused the longer blockage times). Poly-dC$_{100}$, on the other hand, slid right through the nanopore because it had no helical structure. A similar inference could be made from Meller et al about the DNA sequences of poly-dA$_{100}$ and poly-dC$_{100}$ (Meller, Nivon et al. 2000) because of the differences of their blockage currents and times. Our data, however, did not indicate this clear distinction between poly-dC$_{100}$ and poly-dA$_{100}$. There was significant overlap of the current during blockage. Though our data did show that poly-dA$_{100}$ was more likely to spend longer times inside the nanopore. This is consistent with the fact that adenines have greater base-stacking interactions than cytosines, which have the least of DNA bases (Cantor and Schimmel 1980). Couple this fact with the fact that

high concentrations of salt (> 0.3 M) drive complimentary strands of DNA into a helical structure, one molar salt and strong base-stacking interactions may have driven poly-dA_{100} into a helical structure. This helical structure would account for the longer blockages and lower currents. The other regions of blockages may be those molecules of poly-dA_{100} that do not form a helical structure or a partial one.

3.2. *DNA translocation through solid-state nanopores not observed*

Now that we readily observed the translocation of short, single molecules of DNA through individual protein pores, we endeavored to perform identical experiments with the solid state pores. First, two important questions had to be answered: (1) can we mount the nanopore chips in a way that prevents any leakage around the chip edges ? (2) If so, can we estimate the pore size from the measured current? The answer to both questions is "yes."

The solid-state nanopore could be mounted into its chamber and firmly sealed into place within an hour. Once connected to the amplifier, currents were detectable that were comparable in noise to the currents measured in the α-hemolysin nanopore. We performed a critical "bubble test" to verify that current was passing through the nanopore only and not around the sealant. The "bubble test" entailed carefully placing an air bubble across the nanopore to block current flow. If current flow was still detected, then there was a leak. When there was a good seal, the 'bubble test" reduced current to <20 pA (figure 16). Figure 16 also reveals that the typical current through the nanopores was very similar at the same bias voltage as that observed for the membrane-bound protein pores. Thus most of the nanopores were in the predicted 2-5 nm diameter range.
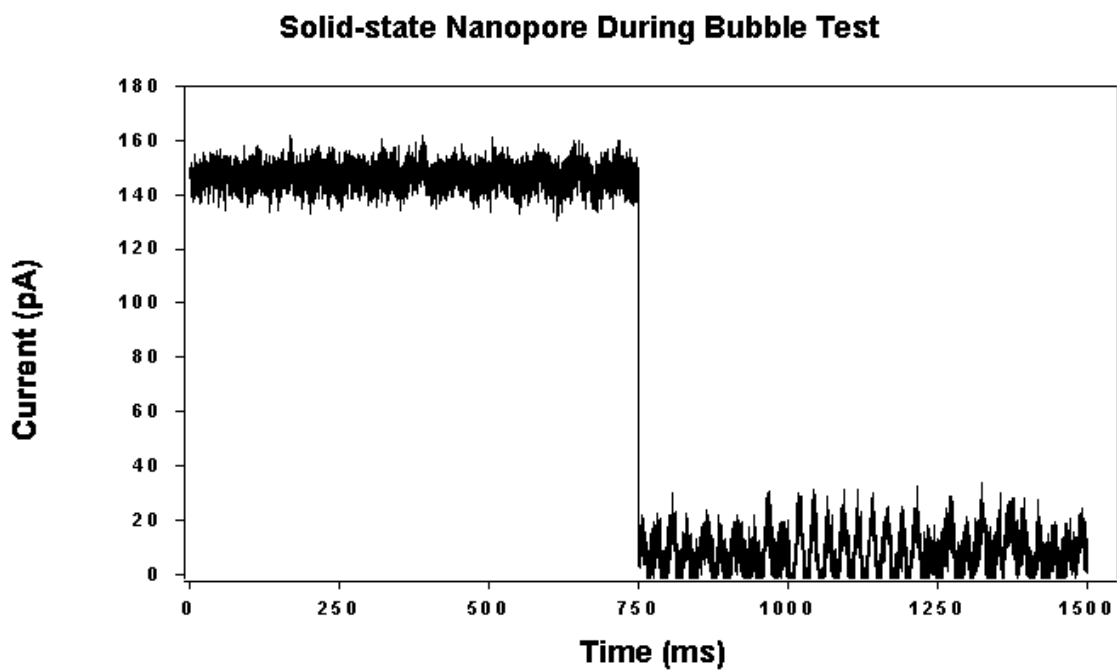
Solid-state Nanopore During Bubble Test

Figure 16. The current through a solid-nanopore chip was comparable to the current through a single α-hemolysin pore at the same voltage (+120 mV). The "bubble test" indicated that the current was through the nanopore and not around the seal. The buffer contained 1 M KCl, 10 mM HEPES at pH 8.

Unfortunately, however, addition of single-stranded DNA to the *cis* reservoir never resulted in detectable current blockages. This disappointing result was the case regardless if the DNA added to the wide side or narrow side of the nanopore (see figures 6,7). We looked for indirect evidence of translocation by looking for detectable DNA on the opposite sides of the nanopore by using unlabeled DNA (measured absorbance at 280 nm) or using fluorescein-labeled DNA (detection done by excitation at 490 nm and measuring the emission spectrum).

Once DNA was not found to translocate through the nanopore, we wondered if the nanopore was partially blocked by debris. We then tried to remove any debris by a piranha wash (5:1 sulfuric acid/hydrogen peroxide), a 30-minute (minimum) overflow rinse in nanopure water, air drying, followed by a 15-minute exposure in an ozone oven. However, this treatment resulted in the same end result; no DNA was detected on the opposite side of a nanopore after lengthy measurements (180 minutes).

We next wanted to get an idea how the membrane surface around the nanopore looked, and possibly get an image of the nanopore. We therefore captured transmission electron microscopy (TEM) images of the surface around the nanopore. TEM indicated at times that some of the nanopore chips had several regions that appeared to contain nanopore-like structure that were 2 – 5 nm diameter; other times there were no indications of nanopore structures. Overall. TEM imaging was very difficult and we pushed the resolution limits.

It is very possible that our results could be explained by the presence of multiple pores in the nitride membrane that were < 1nm diameter, hence unresolvable by TEM. These multiple nanopore structures would together allow a total current to pass that

appeared to come through one larger >2 nm pore, and yet are too small for any one to permit DNA translocation. Furthermore, if DNA did happen to translocate through one pore, it may not have made a noticeable reduction in the total current through all the pores.

Assuming that we had only one nanopore per membrane, we then made attempts to enlarge the pore to improve our chances of seeing DNA translocations. We did this by exposing the solid-state nanopore to hydrofluoric acid (HF) and water mixtures at 1:5, 1:7.5, 1:10 ratios and 1-, 2-, and 5-minute intervals. At the 1:5 and 1:7.5 ratios we found that these were too concentrated in HF. These concentrations resulted in cracks in the membrane (detected by visual inspection under a microscope at 50x magnification). At 1:10 HF to water ratio, we found that exposing the solid-state nanopore for 2 minutes resulted in what appeared to be multiple pores.

Next we wondered if the negative charge of the phosphate group was somehow preventing the DNA from passing through the nanopore. We therefore devised a fluorescent assay to look at the ionic flow through the nanopore. The assay entailed using the fluorescent probe calcein that is negatively charged at pH 8 (the pH of the buffer), and positively charged cobalt ions (cobalt chloride) that quench the fluorescence of calcein. Each constituent of the assay was placed in a well and the voltage was oriented such that the calcein was always on the negative side of the chamber and the cobalt ions were on the positive side. After three hours at +480 mV bias across the nitride membrane, we could see that the side with calcein in it had turned orange in color, as it should when cobalt mixes with calcein. However, the well that contained the cobalt ions at the start of the experiment never changed color; it remained purple (the color of

cobalt chloride in solution). To confirm that calcein did not pass through the nanopore, we measured the absorbance measurements of all samples at 490 nm (the wavelength of maximum of absorbance for calcein). Absorbance measurements for cobalt samples (positive well) showed no absorbance at 490 nm, confirming that calcein did not pass through the nanopore. However, emission spectral measurements showed that cobalt ions passed through the nanopores because the emission spectra showed a reduced intensity (figure 17).

This suggested that only positively charged particles would pass through the nanopore. We therefore looked for current blockages using fluorescein-labeled poly-L-lysine (positively charged protein). We set up the experiment so that poly-L-lysine was placed on the *trans* side of the chamber (the positive electrode) and monitored translocations at +240 mV for 30 minutes or longer. Unfortunately, there still were no detectable current blockages of the nanopore. However, fluorescence and absorbance (490 nm) measurements did show that the poly-L-lysine (p-L-L) passed through the pore to the *trans*-side (figure 18).

In summary, the lack of detectable translocation through the solid-state nanopores was very disappointing. All indications were that we created good leak-free seals around the chips and that the ion current sensitivity was comparable to the single protein pore translocation experiments. We thermally annealed several chips in case the nitride membrane was charged; no success. At this point the only conclusion that we can form is that multiple nanopores were present.
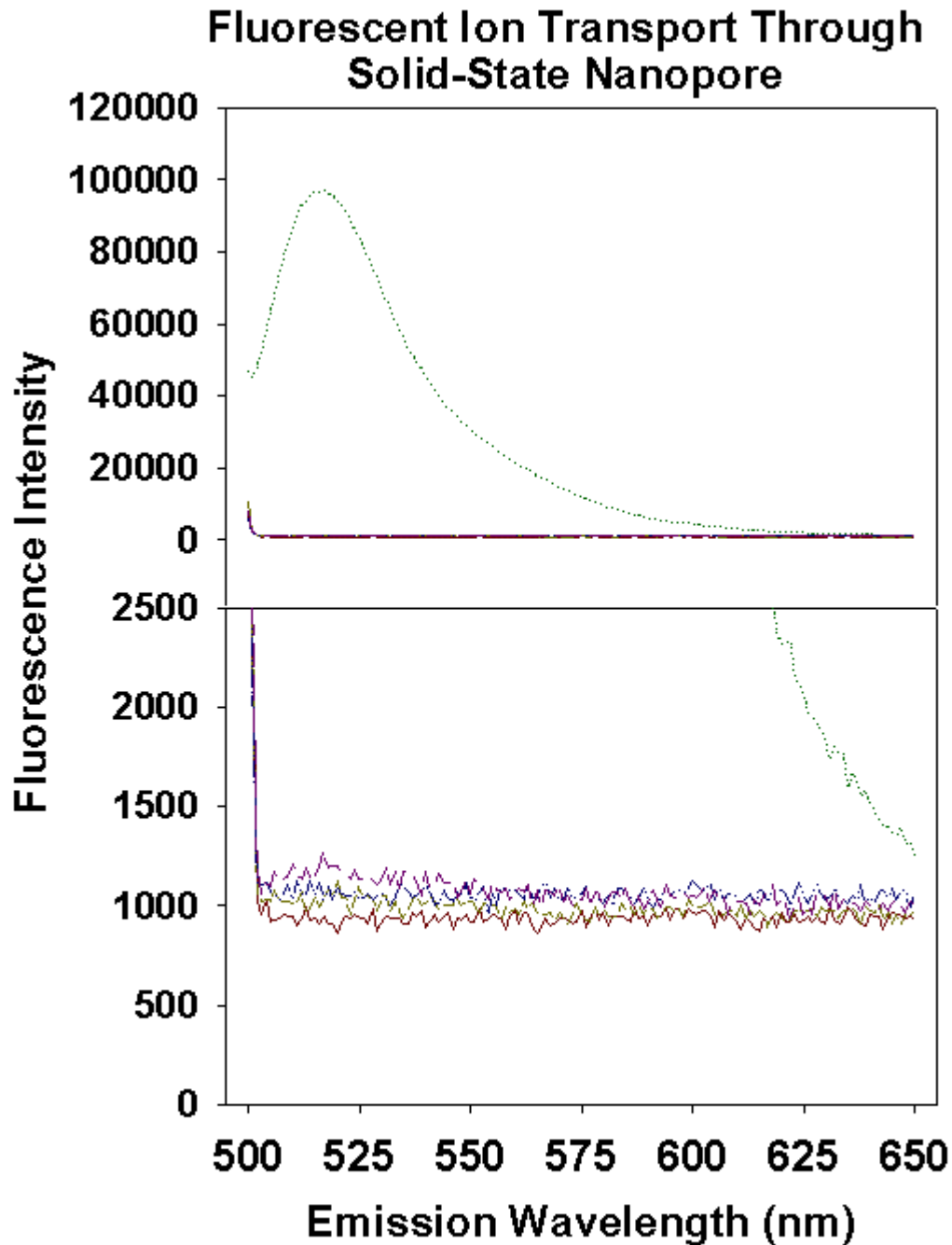
Figure 17. The fluorescent probe calcein was used to monitor ionic flow through a solid-state nanopore. Calcein was negatively charged at pH 8. Cobalt chloride was the quenching agent. At +480 mV, only cobalt was found to migrate from one side (positive) to the other (negative). The bottom of the figure is a blow-up of the top section.
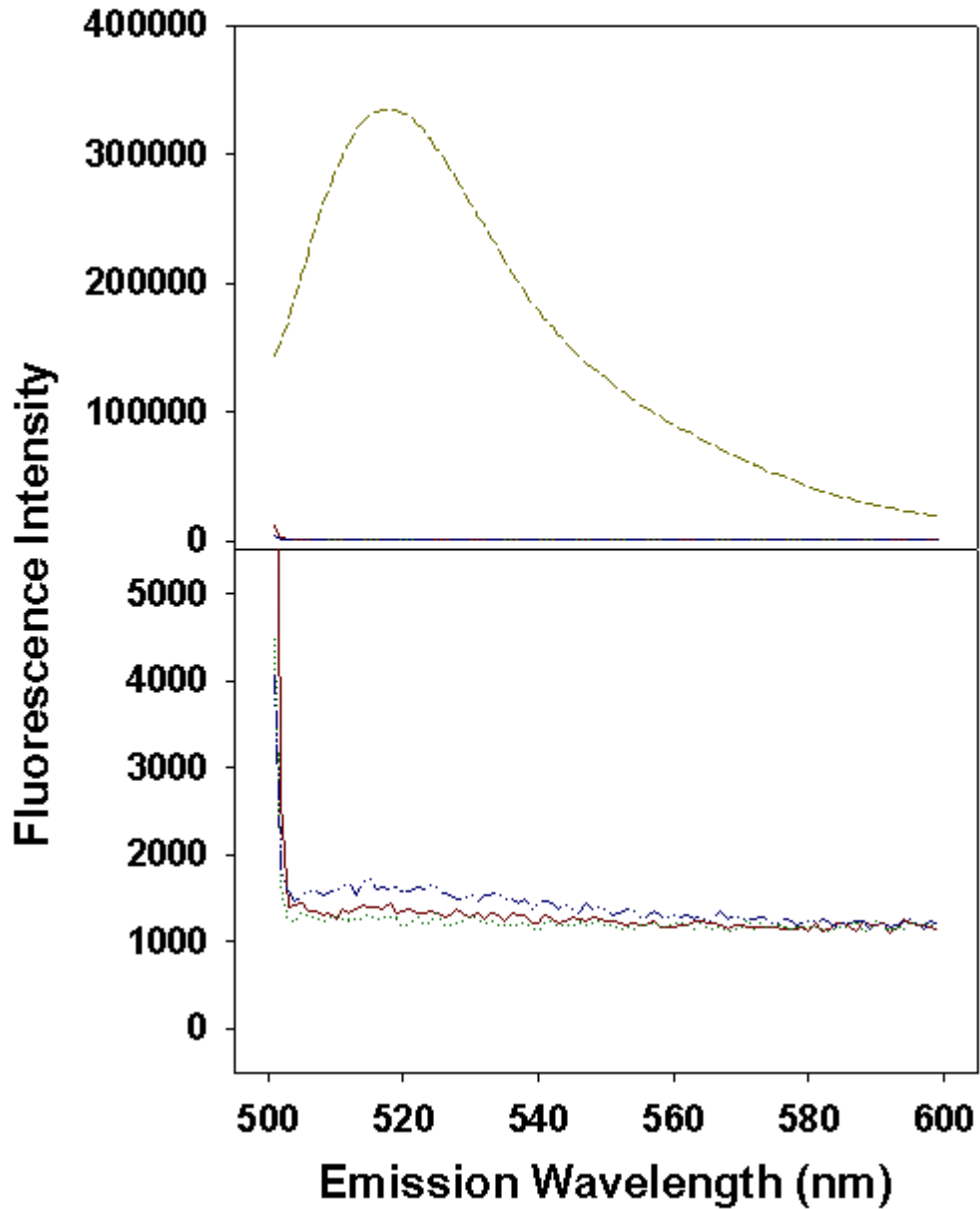
Figure 18. Fluorescent-labeled poly-L-lysine, a positively charged polymer, was used to monitor polymer migration through a nanopore chip. Poly-L-lysine was found to migrate to the opposite side of the nanopore when +240 mV was held across the nanopore (blue curve). The bottom portion is a blow-up of the top section.

3.3. *Nanopore formation by Tetanus toxin*

Leveraging our capability to detect single protein pores, we performed some pH dependence experiments on the pore-forming activity of tetanus toxin. Since tetanus toxin binds to GT1b receptors, we first had to test whether a lipid system containing the ganglioside GT1b would readily form a stable bilayer. Our first attempts were done with the lipid components of 95-mol% DPh-PC and 5-mol% GT1b (DPh-PC worked well for the α-hemolysin studies discuss above). We then tried DSPC/chol/GT1b at 47.5/47.5/5 mol% (lipid system chosen to keep conditions the same as those in some concurrent atomic force microscopy experiments). The buffer was 150 mM NaCl, 5 mM citrate-HEPES-MES, at pH 7.4 (or 4) ± 0.05.

Both bilayer systems formed stable, thin (transient spikes ~ 2000 pA) bilayers for 30 – 60 minutes in 150 mM NaCl, at pH 7.4 (and pH 4) and 120 mV. The bilayer system containing DPh-PC formed a thin bilayer within 15 minutes, using the standard solvent hexadecane. However, bilayers of DSPC/cholesterol/GT1b took longer (30–60 minutes) to form, and required a solvent mixture of decane and hexadecane.

Atomic force microscopy images indicated that tetanus C-fragment (Tet-C, the portion of the heavy chain that contains the binding site for GT1b, ~ 50 kD in size) bound to the bilayer of 1:1 dipalmitoyl phosphatidylcholine/dipalmitoleoyl phosphatidylcholine with 10% GT1b at pH 7.4 after ~2 hours of incubation. However, defects (~40 - 80 nm in diameter) formed in the bilayer after ~ 12 hours. Therefore, our next step was to evaluate the pore formation activities of Tet-C in DPh-PC/GT1b (95:5 mol%) bilayer. Initial current measurements showed that at least one pore (most likely several pores) formed about one hour and 45 minutes after adding ~ 0.65 µg Tet-C (4.06 µg/ml; we used 13-

times the amount required for the α–hemolysin experiments because a single tetanus pore is much smaller, ~ 1–8 pA/tetanus pore vs. 120 pA/α–hemolysin pore) to the *cis*-well. This was unexpected since all of the literature on pore formation of Tet-C suggested that Tet-C did not form any nanopore structures. Therefore, we analyzed our samples of Tet-C for purity by gel analysis. Size exclusion gel analysis showed that our stock Tet-C contained light bands of contaminants approximately in the size range of the full heavy chain of tetanus (~100 kD) and the full tetanus toxin (~150 kD) (figure 19). This would explain the unexpected results of pore formation with the Tet-C sample. Small amounts of tetanus heavy chain and/or full toxin in a 20-μg stock solution of Tet-C are more than enough contaminants to form pores (it takes 20 – 50 ng of α-hemolysin to form a pore).

We thus evaluated the pore forming properties of the full tetanus toxin (150 KD) in the DSPC/chol/GT1b and DPh-PC/GT1b bilayers as a function of pH. For the DSPC/chol/GT1b bilayer and 125 ng/ml full tetantus concentration at +120 mV, bursts (not continuously open) of pores formed with a maximum current around 50 pA (figure 20). As the concentration was increased to 250 and 500 ng/ml the frequency of pore formation (bursts) reduced over a 30-minute period. The reduced pore formation rate at higher concentration of full tetanus toxin implied that tetanus might form aggregates in solution. This was confirmed by dynamic light scattering data that showed tetanus particle size increasing with increased concentration. The particle size of tetanus was also pH-dependent; for > 1.67 μg/ml, the aggregate size at pH 4 was nearly twice that of aggregates at pH 7.4 (figure 21). However, no pores formed at pH 4.

Tetanus fragment-C gel with 3 impurity bands

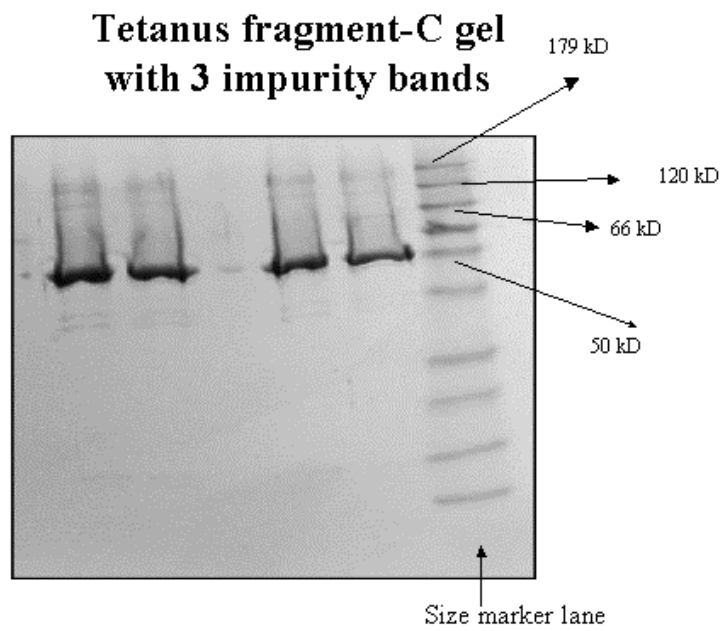179 kD

120 kD

66 kD

50 kD

Size marker lane

Figure 19. SDS-Gel of the tetanus C-fragment showed contamination of the stock solution. Tetanus C-fragment is the dark band around 50 kD. The other two bands are near the size of the heavy chains (~100 kD) and full toxin (~150 kD).
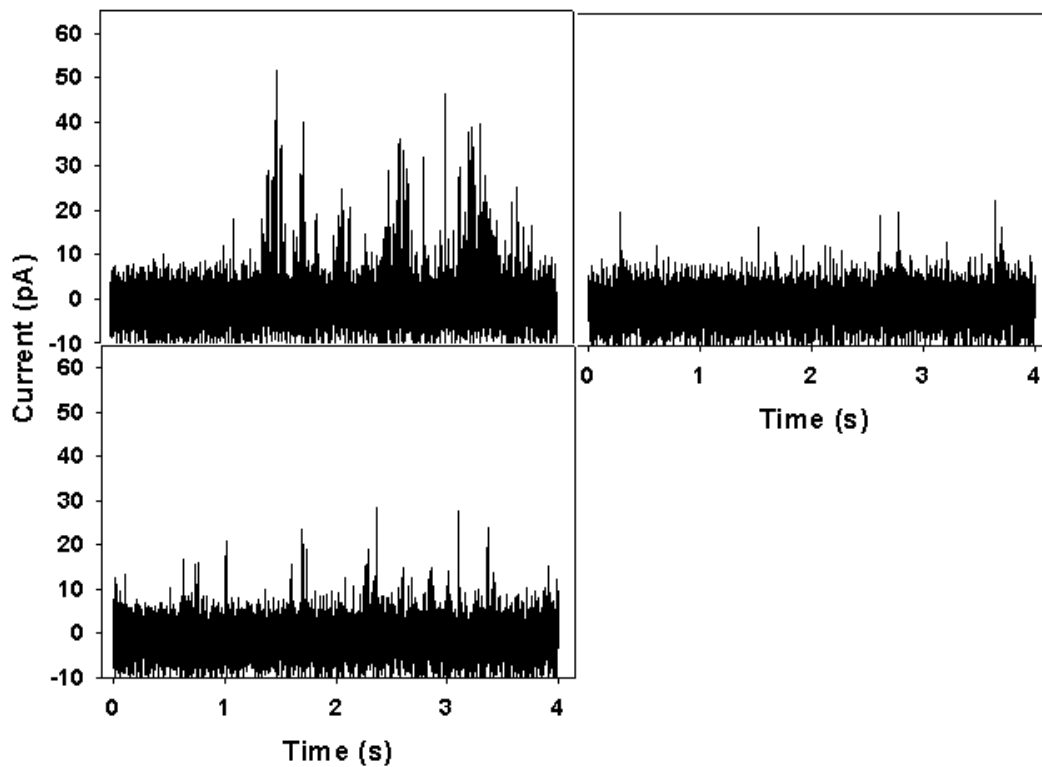
Figure 20. Tetanus toxin formed pores in DSPC/cholesterol/GT1b (47.5/47.5/5 mol%) bilayer. Pore activity appeared to decrease with added toxin concentration.
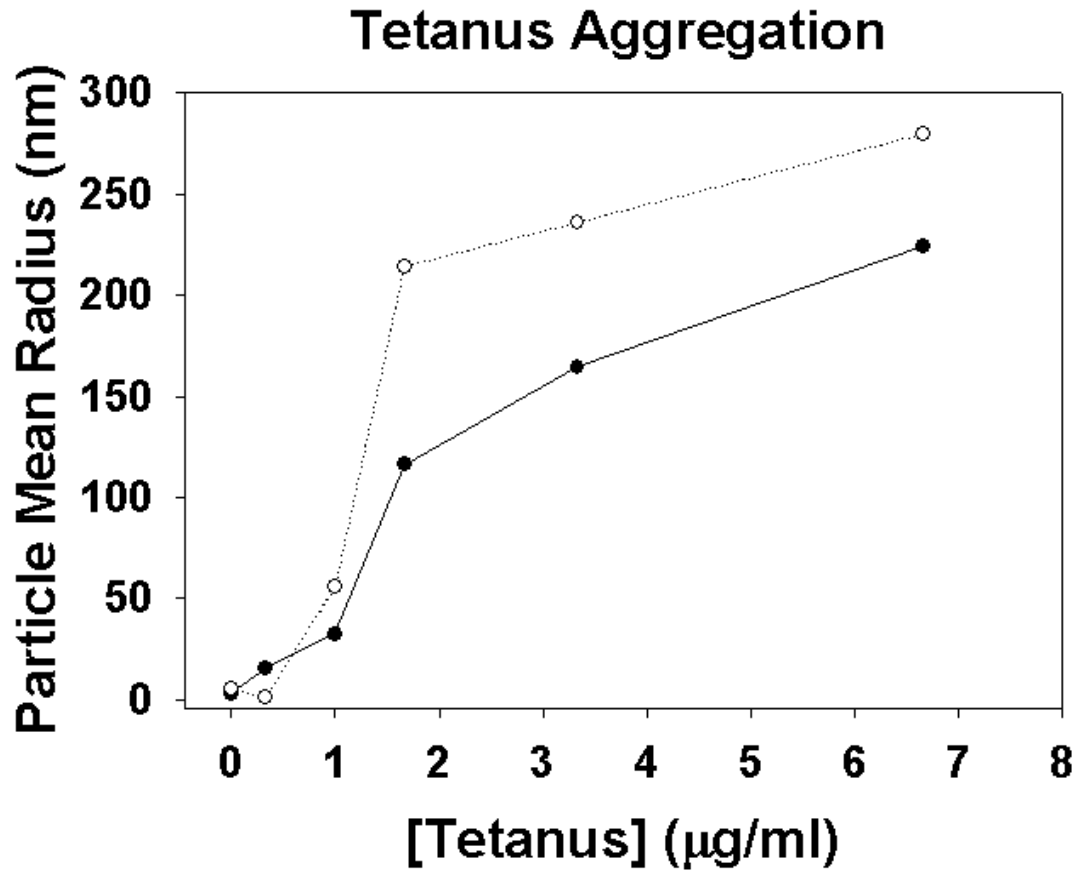
Figure 21. Tetanus aggregation is pH-dependent. Tetanus aggregates in solution at 1.67 µg/ml were twice as big at pH 4 than at pH 7.4.

Upon adding tetanus at ~5 µg/ml to DPh-PC/GT1b (95/5 mol%) at pH 7.4, pores readily formed. The pores were opening and closing more frequently than at the lower concentration in the DSPC/chol/GT1b bilayer system. At 120 mV and 150 mM NaCl, the pores had a maximum current peak around 120 pA. As in the other bilayer system, there was no pore formation at pH 4 in the DPh-PC/GT1b system (figure 22).

4.0 Summary

Starting from scratch in this project we established the capability to detect a single protein nanopore forming in a leak-free bilayer system. We have also demonstrated that we can characterize the translocation dynamics of single-stranded DNA 100 bases in length. In particular, we were able to show that poly-dA$_{100}$ exhibited 3 distinct populations of blockages that were somewhat different than the blockages exhibited by poly-dC$_{100}$. In our research, we showed that we could also alter the blockage pattern of poly-dC$_{100}$ by the introduction of poly-dT$_{25}$, a more distinctive pore-blocking DNA sequence. As for the ability to mimic this process in a solid-state nanopore, we have demonstrated that we presently only can achieve the same current sensitivity. Blockages by single strand DNA were not observed. As for toxins like tetanus, we also have the capabilities to study them in the presence of leak-free bilayers and as a function of physiological conditions. We have demonstrated that tetanus does form pores in two different bilayer systems at pH 7.4, but not pH 4.

The next question that arises is: Where do we go from here? With further efforts, we should have the capabilities to distinguish multiple analytes in solution using a single

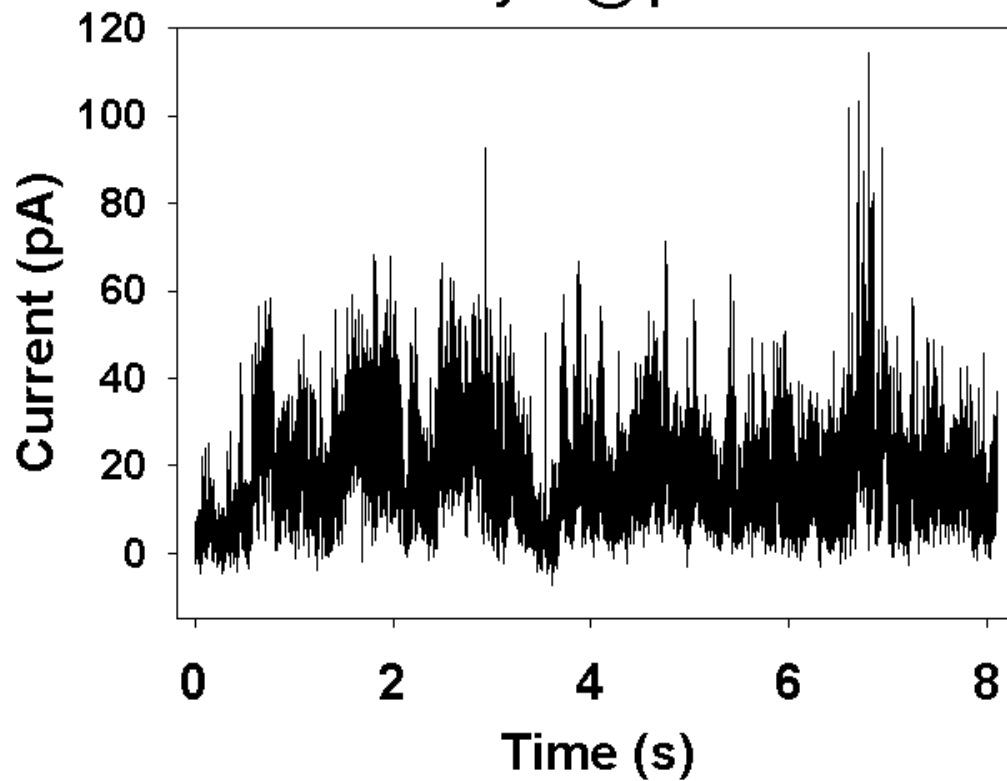**Tetanus Toxin in DPh-PC/GT1b (95/5 mol%) Bilayer @ pH 7.4**

Figure 22. Tetanus toxin formed pores more readily at 5 μg/ml in DPh-PC/GT1b (95/5 mol%) bilayer at pH 7.4. Current peaked around 120 pA at +120 mV and 150 mM NaCl.

α-hemolysin nanopore. This may entail refining our electronics so that it can give us better time resolution for sequence-dependent dynamics .

To better understand the dynamics of single-stranded DNA we should continue this research carefully exploring the affects of temperature, salt concentration, and applied voltage has on structure. One or a combination of these conditions may significantly change the structure of the molecule such that it slows down as it passes through a protein nanopore, thereby possibly increase resolution at the same time.

Concerning the solid-state nanopore, we need to simplify the overall design and fabrication process. We could do that by limiting the material of the nanopore chip to one material, and varying the diameter of the nanopore. This would allow us to accomplish two things. First, this would allow us to understand how one material may affect a polymer without complicating the physics with multiple dielectric regions. Secondly, the larger nanopore would give us a better frame of reference to which to compare smaller nanopores.

5.0   References

Akeson, M., D. Branton, et al. (1999). "Microsecond Time-Scale Discrimination Among Polycytidylic Acid, Polyadenylic Acid, and Polyuridylic Acid as Homopolymers or as Segments Within Single RNA Molecules." Biophys. J. **77** (6): 3227-3233.

Cantor, C. R. and P. R. Schimmel (1980). Biophysical Chemistry, Part III: The behavior of biological macromolecules. New York, NY, W.H. Freeman and Company.

Kasianowicz, J. J., E. Brandin, et al. (1996). "Characterization of individual polynucleotide molecules using a membrane channel." Proceedings Of The National Academy Of Sciences Of The United States Of America: 13770-13773.

Kasianowicz, J. J., S. E. Henrickson, et al. (2001). "Simultaneous multianalyte detection with a nanometer-scale pore." Anal Chem **73** (10): 2268-72.

Liu, H. I., D. K. Biegelsen, et al. (1993). "Self-Limiting Oxidation for Fabricating Sub-5 nm Silicon Nanowires." Applied Physics Lett **64** (11): 1383 - 1385.

Meller, A., L. Nivon, et al. (2000). "Rapid nanopore discrimination between single polynucleotide molecules." PNAS **97** (3): 1079-1084.

Movileanu, L., S. Howorka, et al. (2000). "Detecting protein analytes that modulate transmembrane movement of a polymer chain within a single protein pore." Nature Biotechnology: 1091-1095.

Song, L., M. R. Hobaugh, et al. (1996). "Structure of Staphylococcal alpha -Hemolysin, a Heptameric Transmembrane Pore." Science **274** (5294): 1859-1865.

DISTRIBUTION

3	MS1413	A. R. Burns, 1141
1	MS1413	P. V. Dressendorfer, 1141
1	MS1415	B. S. Swartzentruber, 1114
1	MS1080	J. G. Fleming, 1749
1	MS0188	LDRD Office, 10300
1	MS9018	Central Technical Files, 8945-2
2	MS0899	Technical Library, 9616